Comparison of erosion and deposition in JET divertor during the first three ITER-like wall campaigns

S Krat[1,2] ⬤, **M Mayer**[2] ⬤, **A Baron-Wiechec**[3], **S Brezinsek**[4] ⬤, **P Coad**[3],
Yu Gasparyan[1], **K Heinola**[5] ⬤, **I Jepu**[6], **J Likonen**[7], **P Petersson**[8], **C Ruset**[6],
G de Saint-Aubin[2], **A Widdowson**[3] ⬤ **and JET contributors**[9]

[1] National Research Nuclear University MEPhI, Moscow, Russia
[2] Max Planck Institute for Plasma Physics, Garching, Germany
[3] Culham Centre for Fusion Energy, Culham Science Centre, Abingdon, United Kingdom
[4] Forschungszentrum Jülich GmbH, Jülich, Germany
[5] University of Helsinki, Helsinki, Finland
[6] National Institute for Laser, Plasma and Radiation Physics, Bucharest, Romania
[7] VTT Technical Research Centre of Finland, Finland
[8] Fusion Plasma Physics, Royal Institute of Technology, Stockholm, Sweden

E-mail: sakrat@mephi.ru

CrossMark

Abstract

The manuscript presents an overview of the erosion and deposition data in the inner and outer JET divertor observed during the first three ITER-like wall campaigns (JET-ILW1, JET-ILW2, JET-ILW3). Erosion and deposition were studied using core samples cut out from divertor tiles. For the studied samples a similar general deposition pattern was observed in all three campaigns: More than 60% of the total deposition occurred in the upper region of the inner divertor on tiles 0 and 1, where Be was transported and deposited from the scrape-off layer. High erosion was observed only on tile 5. In JET-ILW2 and 3, erosion together with high power fluxes was observed in the outer divertor at the bottom of tile 7. Additionally, deposition peaks were observed on the sloping parts of tiles 4 and 6, which were more pronounced in JET-ILW2 and 3 due to placing the strike point more often on these tiles. The deposits consisted primarily of Be, with some additional D and C. Deposition rates were observed to decrease from campaign to campaign, with the C deposition rate decreasing the most, more than 2 times from JET-ILW1 to JET-ILW3. D retention up to levels of $\sim$1 at% was observed up to large depths in the W protective coatings in all campaigns.

(Some figures may appear in colour only in the online journal)

1. Introduction

Erosion of plasma facing components of fusion devices is one of the primary threats for their long-term functionality. Erosion limits component lifetime, while during the plasma discharge eroded material might be introduced into the core plasma, leading to significant increase in radiative cooling and lowering the plasma temperature. Redeposition of eroded material can lead to the formation of hydrogen-rich layers [1, 2], which is a potential significant issue from the viewpoint of tritium inventory as well as hydrogen recycling during the discharge. Redeposited layers often have significantly different physical properties compared to their substrates, leading to changes in plasma-wall interaction and

[9] See the author list of E Joffrin et al 2019 Nucl. Fusion **59** 112021

Table 1. Some parameters of the first three JET-ILW campaign.

Campaign	Period	Total plasma time (h)	Input energy (GJ)	Characteristics	Comments
JET-ILW1	2011–2012	19.1	150	Low power D plasmas	
JET-ILW2	2013–2014	19	201	Higher power D plasmas	Finished with 300 discharges in H
JET-ILW3	2015–2016	23.5	245	D plasmas	Finished with N_2 seeded H mode for 0.25 h
				H plasmas D plasmas (high power)	

plasma performance over time. Formation of thick redeposited layers can lead to flaking and dust formation. In order to be able to predict the long-term behavior of a fusion device, the study of erosion and deposition, as well as the study of the transport of eroded material is an important task.

During JET operation with all-carbon walls prior to 2010 (JET-C) massive redeposition mainly of carbon was observed in the whole inner divertor, parts of the outer divertor, and in remote divertor areas [1, 3]. Re-deposited layers with thicknesses of more than 500 μm were observed [1]. This massive carbon deposition was accompanied by a high retention of hydrogen isotopes trapped by co-deposition, resulting in the formation of hydrocarbon layers with high hydrogen concentrations.

In 2010, the plasma-facing components of JET were changed from full carbon to the ITER-like wall (JET-ILW) configuration, comprising of Be tiles in the main chamber and carbon tiles coated with thick ($\sim$20 μm) W layers in the divertor [4] with a bulk W central divertor tile [5]. The JET-ILW was shown to affect the erosion-deposition patterns [6–9] and fuel retention [10] as compared to the previous full carbon device.

The first three JET-ILW campaigns (JET-ILW1, JET-ILW2, and JET-ILW3) all had progressively more powerful and varied plasma discharges, as well as differing strike-point distributions, and represent the typical range of plasma shapes and conditions with JET-ILW; some integral campaign parameters are shown in table 1. As such, it is important to compare the erosion-deposition patterns in the divertor for the three campaigns, in order to ascertain commonalities and differences and discern long-term trends introduced by the change to the JET-ILW configuration.

This paper presents an overview of the erosion and deposition data in the inner and outer divertors of JET during the first three ILW campaigns, and compares them, focusing on explaining the differences between erosion and deposition in the three campaigns.

2. Experimental

2.1. Analyzed tiles

In order to study surface erosion, a number of divertor tiles have been coated with tungsten 'marker layers'. On top of the

tile surfaces, a $\sim$3 μm thick molybdenum coating was deposited. On top of molybdenum coating, a $\sim$3 μm thick tungsten coating was deposited. The same coating technology as the one used for producing the tungsten protective coating for the whole divertor was used, so the structure of the tungsten marker layers was similar to the structure of other divertor tiles' surfaces. Additionally, several tiles were produced with molybdenum coating only, in order to study tungsten transport and redeposition in the divertor. These were tile 3 in JET-ILW1 and tile 4 in JET-ILW2 (see figure 1 for a schematic representation of the JET-ILW divertor). Full poloidal sets of tiles with marker coatings were installed in the JET divertor in all campaigns. Tiles 0, 3, 7 and 8 were installed in the JET divertor both for JET-ILW1 and JET-ILW2, and studied after the end of JET-ILW2. In order to obtain erosion and deposition data for JET-ILW2 for those tiles, data from JET-ILW1 were deducted from the measured erosion and deposition values.

Tiles 1, 4 and 6 removed after JET-ILW3 did not have marker coatings, and so erosion on their surfaces could not be studied.

After the experimental campaigns tiles were removed and cylindrical 'core samples' were cut out. The core samples were $\sim$16 mm in diameter. The distance between the centers of neighboring core samples was 20 mm in poloidal direction (along the 's-coordinate' axis used in the JET divertor). On each core two points were analyzed, 8 mm apart, and each 4 mm away from the center of the core sample's surface.

Additionally, after JET-ILW1 and JET-ILW2, sets of tungsten lamellae from tile 5 were removed and studied. Because tile 5 was toroidally asymmetric, several sets of lamellae were removed—from lines 2, 3, 13, 14, 22, and 23. Of those, lamellae from lines 2, 13 and 22 were coated with W marker layers.

2.2. Ion beam analysis

Prior to their installation inside JET, the thicknesses of marker layers, including thicknesses of Mo interlayers, were measured (pre-characterized) using elastic backscattering (EBS) with 3 MeV protons in the BOMBARDINO/BesTec setup, which allows nondestructive analysis of whole non-contaminated tiles. The uncertainties for the determination of the changes of layer thicknesses are about 160 nm for the top W layer and about 320 nm for the Mo interlayer.
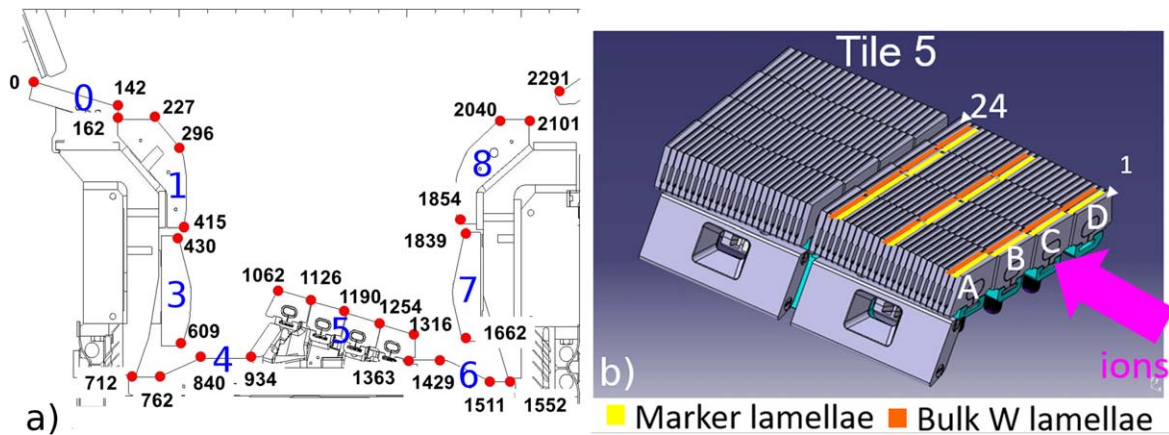
Figure 1. (a) Cross-section of the JET-ILW divertor. Coordinates in the divertor are measured using the *s*-coordinate system with the origin at the inner corner of tile 0. Red dots indicate characteristic points of divertor tiles; black numbers indicate coordinates of those red dots in the *s*-coordinate system (in mm) directed along the surfaces of the tiles; blue numbers indicate tile numbers. (b) Schematic drawing of tile 5 of the JET-ILW divertor: white numbers and letters indicate rows and lines of bulk W lamellae. Orange lines indicate lamellae without W marker layers that were analyzed during JET-ILW1, yellow lines—marker coated lamellae that were analyzed.

After the end of the experimental campaign, several ion beam diagnostics were used to study near-surface areas of tiles.

Tungsten and molybdenum marker layer thicknesses as well as the amounts of beryllium, carbon and oxygen in thick deposits were determined using EBS with 3 MeV protons, similar to the pre-characterization analysis. For tiles 0 and 1, where very thick deposits were observed, in addition 3.8 and 4.5 MeV incident protons were used. A PIPS detector was located at a scattering angle of 165° in the laboratory system with an experimentally measured solid angle of (1.72 ± 0.02) msr. The total charge per measurement was 2 μC, which corresponds to several thousands of counts per channel in the obtained spectra. Incident proton energies were high enough that the thicknesses and compositions of (thick) deposited layers, the W marker layer, and the Mo interlayer could be determined.

Non-Rutherford scattering cross-sections were used for the analysis of the Be [11], C[12], and O [12] signals. In regions with thick deposits, the total amounts of Be, C and O were calculated based not only on the signals of their peaks, but also on the shift of the W high-energy edge. The roughness of the deposited layer was calculated based on the slope of the W edge.

Nuclear reaction analysis (NRA) was used to measure the amounts of D, Be and C. 1.0 and 2.4 MeV ^{3}He$^+$ ions were used for areas with small amounts of deposits. For areas of thick deposits, as well as in the areas where D depth profiling was performed, 1.7, 3.0, 4.0, 4.5 MeV ^{3}He$^+$ ions were also used. The NRA detector was a 2000 μm thick PIPS detector located at a reaction angle of 135° in the laboratory system with an experimentally measured solid angle of (22 ± 1) msr. The detector has a parabolic slit for minimizing kinematic energy spread [13] and was covered with a stack of 5 μm Ni and 13 μm Mylar foils for filtering backscattered ^{3}He ions. The total charge per measurement was 2 μC.

The D(^{3}He,p)^{4}He reaction was used to measure the D content [14]. The ^{12}C(^{3}He,p$_0$)^{14}N and ^{12}C(^{3}He,p$_1$)^{14}N reactions were used to measure the C content [15]. The ^{9}Be(^{3}He,p$_0$)^{11}B and ^{9}Be(^{3}He,p$_1$)^{11}B reactions were used to measure the Be content [16].

3. Results and discussion

3.1. Erosion

The thicknesses of W marker layers before and after the JET-ILW1, JET-ILW2, and JET-ILW3 campaigns are shown in figures 2(a)–(c), respectively. Additionally, the comparison between thicknesses of Mo interlayers before and after the campaigns are shown. The discrepancies between these values for tiles with W marker layers may be explained by inhomogeneities of the Mo layer itself, measured at different toroidal positions on the tile surface.

In JET-ILW1, one can observe erosion of W near the bottom of tile 1, and strong erosion of the Mo marker layer in the upper area of tile 3, which did not have a W marker layer, but only a Mo layer facing plasma. In the same upper area of tile 3 one can also observe W redeposition, either from tile 1, or from toroidal transport from nearby tiles 3. In JET-ILW2 erosion in the upper area of tile 3 can be observed.

It should be noted that the Mo erosion is much more pronounced than the erosion of W both in the JET-ILW1 and JET-ILW2 campaigns (tile 4 in JET-ILW2), which is indicative of relatively low energy of deuterium particles sputtering the divertor surface—in the inter-ELM periods this energy was estimated as ~200 eV [17], which would mean ~5 times lower sputtering yield of W by D compared to the sputtering yield of Mo by D [18].

Clear deposition of W was observed only in the JET-ILW1 campaign, in the middle of tile 1. In JET-ILW2 and JET-ILW3, no clear indications of W redeposition were observed. Deposition of W was observed on both tiles with no W marker coatings (tile 3 in JET-ILW1 and tile 4 in JET-ILW2), in the areas close to the maximum Mo erosion areas
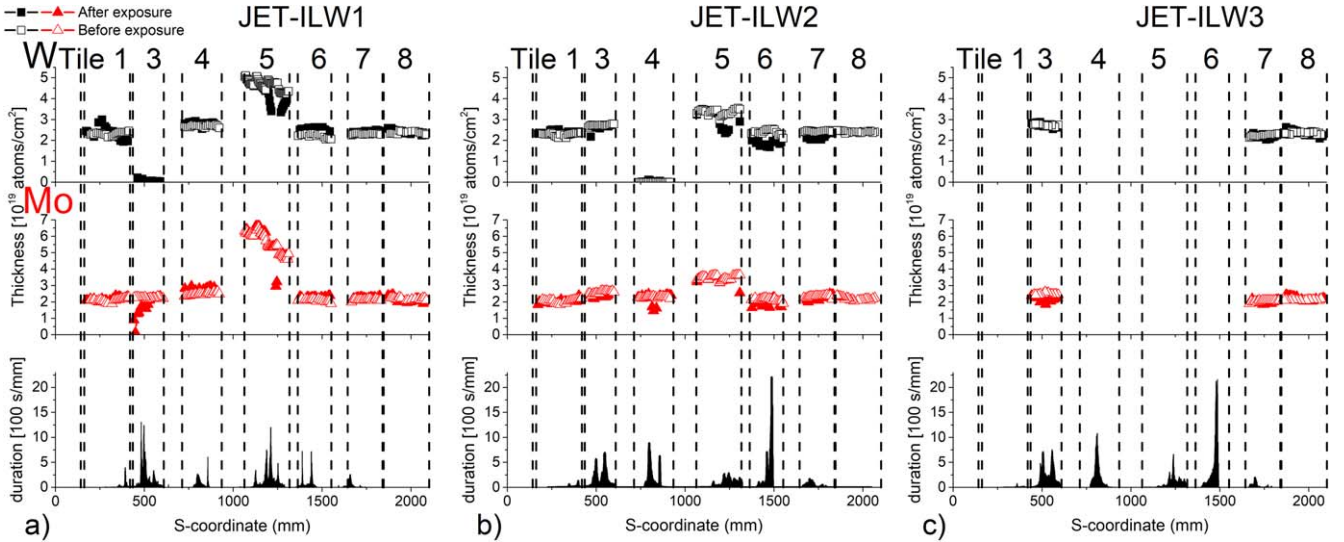
Figure 2. Top to bottom: W (black squares) and Mo (red triangles) thicknesses measured before campaigns (hollow symbols) and after campaigns (filled symbols), and strike point distribution during the campaigns for (a) JET-ILW1, (b) JET-ILW2, (c) JET-ILW3.
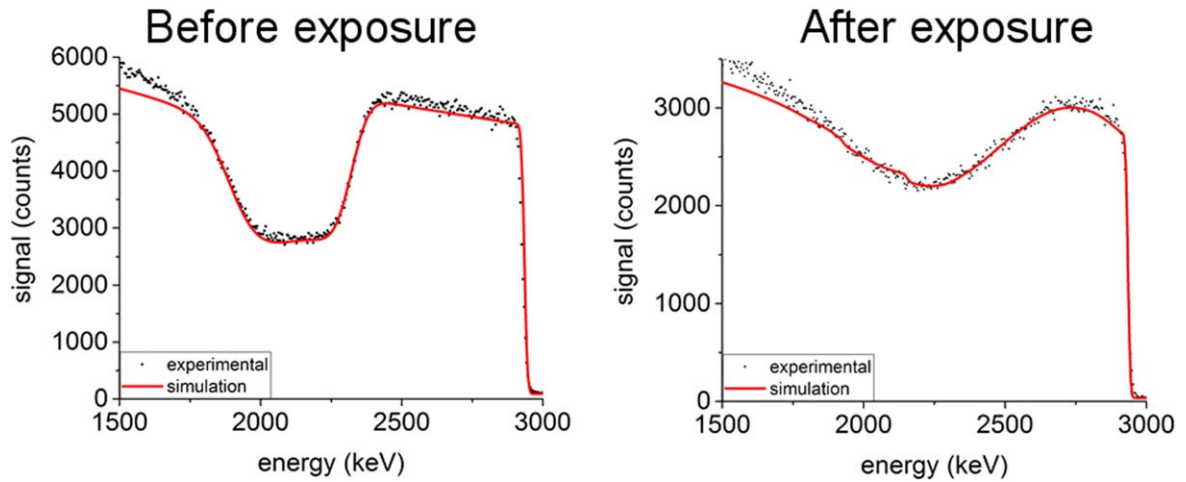

Figure 3. Characteristic shapes of EBS spectra for the lower part of tile 7 of the outer divertor for JET-ILW2 and JET-ILW3. Left—pre-characterization spectra, right—post-mortem analysis. Black dots—experimentally measured data, red line—SIMNRA simulation.

(top of tile 3 in JET-ILW1 and middle of tile 4 in JET-ILW2). This transport could be caused by transport of eroded W in toroidal direction and redeposition on Mo-coated tiles from neighboring W-coated tiles.

In both JET-ILW1 and JET-ILW2 for which data from tile 5 is available, the strongest erosion was observed there, in the areas close to the maximum duration of strike-point positioning. In a number of areas of tile 5, delamination of W marker coating was observed, making it impossible to obtain quantitative erosion data, but indicating high heat fluxes in those areas.

In both JET-ILW2 and JET-ILW3, erosion was observed in the outer divertor, on tiles 6 and 7, near the strike-point position. In JET-ILW1, where strike-points were located far from the outer divertor, no significant erosion was observed in the outer divertor.

In both JET-ILW2 and JET-ILW3, significant changes were observed in the EBS spectra of the area near the bottom

of tile 7 (figure 3). The EBS spectra did not show any clear interfaces between the W marker layer and the underlying Mo interlayer. The smooth transition in the EBS spectra can be indicative of either layer interdiffusion or a strongly inhomogeneous erosion on the microscale leading to a very rough W marker layer. Because a significant amount of D was still present in the W marker layer (see below), which was not observed in the layers of tile 6 which experienced high heat loads and strong heating, but did not show the same smooth EBS spectra, the layer interdiffusion is less likely to be the correct explanation. The increase in the effect correlates well with the amount of erosion observed on the surface of the tile. Assuming roughness to be the correct interpretation, at the bottom of the tile the roughness was approximately equal to the remaining W thickness. A reasonable SIMNRA fit (red lines in figure 3) of the experimental data was achieved by adjusting the layer roughness from $\sim 2 \times 10^{18}$ atoms cm^{-2} (left figure) to $\sim 2 \times 10^{19}$ atoms cm^{-2} (right figure). In
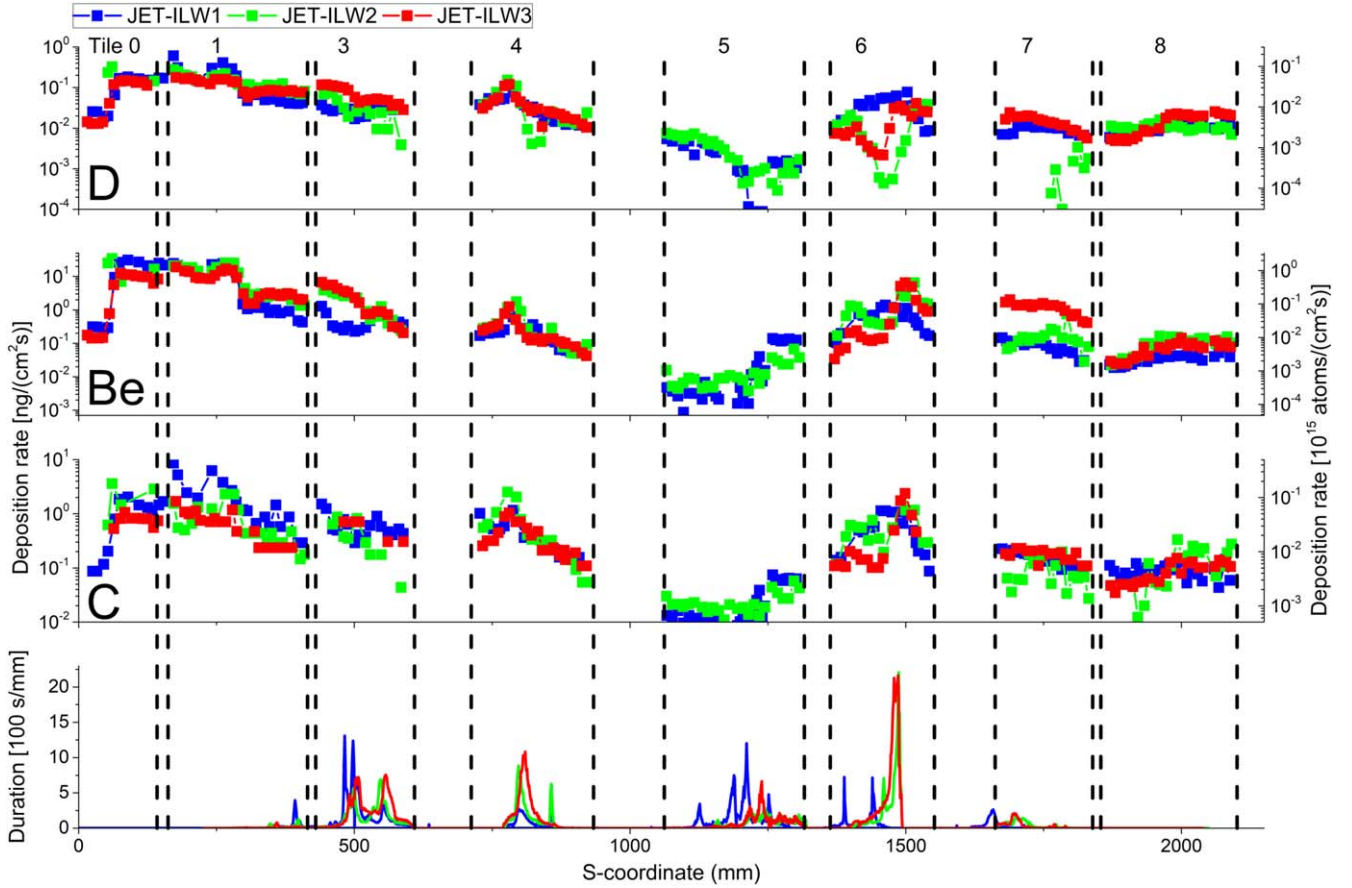
Figure 4. Top to bottom: distributions of D, Be and C deposition rates (in logarithmic scale), and distribution of strike point positions (linear scale) in the first three JET-ILW campaigns. Blue—JET-ILW1, green—JET-ILW2, red—JET-ILW3. Vertical dashed lines indicate borders of the divertor tiles. Black numbers on top of the figure—numbers of the tiles. For tile 5, data is shown for the lamellae in row 13.

JET-ILW1, in which strike-point positions were far away from the outer divertor, no such changes to the near surface layers of tile 7 were observed.

3.2. Deposition

Distributions of the deposition of D, Be and C in the first three ILW campaigns are shown in figure 4, with corresponding distribution of strike point localization durations below them.

One can see that overall in all three campaigns, the distribution patterns were very similar. Most of the deposition is observed in the inner divertor on tiles 0 and 1. This is in contrast to results observed during JET-C, where most deposits were observed on tiles 4 and 6. The difference is likely due to differences in Be and C transport through the divertor. C has a high chemical erosion rate and could be transported through the divertor in a step-by-step process, eroding from one point, re-depositing onto the next one nearby deeper in the divertor, and then repeating this process. Be has a lower erosion rate by D and is not as susceptible to chemical erosion. Because of this, it mostly remains in the area where it is first transported from the scrape-off-layer (SOL) into the divertor.

One can see that for JET-ILW2 and JET-ILW3, where strike point positions where more often on tiles 4 and 6, peaks

of Be deposition are present on those tiles, in the areas corresponding to the central sloped parts. At the same time, the D content on tiles 4 and 6 is lower for JET-ILW2 and JET-ILW3, likely due to higher peak surface temperature of the tiles during those campaigns. In areas where very high temperature ($T \sim 1400$ K) were observed [19], almost no deuterium was found.

The Be deposition rate was about 3 times higher on tile 7 during JET-ILW3 than during JET-ILW2, and about 5 times higher than during JET-ILW1. This is explained by the difference in the outer strike point distribution. During JET-ILW3 the strike point was often position on tile 6, so the lower area of tile 7 experienced significant fluxes from the SOL, resulting in a higher Be accumulation rate.

In JET-ILW3, where also N_2 puffing was employed, N was observed in the areas of highest deposition (tiles 0 and 1). In the same areas, oxygen was observed, possibly due to oxidation of Be layers after contact with atmospheric air.

The total amounts of D, Be and C accumulated in JET divertor during the first three JET-ILW campaigns are shown in table 2.

One can see that the accumulation of C underwent the most significant reduction from campaign to campaign both in terms of the absolute amount of C accumulated and in terms of accumulation rates. The relatively high C accumulation
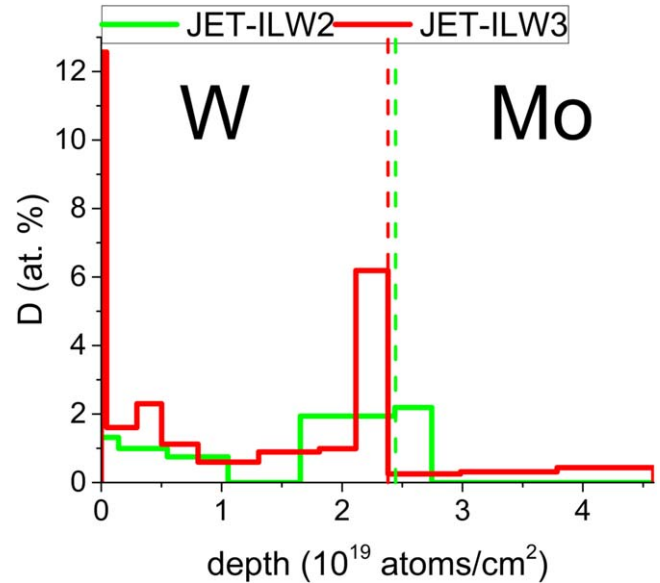
Table 2. Total amounts and rates of D, Be and C accumulation in JET divertor during JET-ILW1, JET-ILW2, and JET-ILW3 campaigns.

	JET-ILW1	JET-ILW2	JET-ILW3
D, g	0.9	0.7	0.9
D, μg s^{-1}	13	10	11
D, μg MJ^{-1}	6.0	3.5	3.7
D, μg W^{-1}	0.41	0.24	0.31
Be, g	53	60	46
Be, μg s^{-1}	771	877	544
Be, μg MJ^{-1}	353	299	188
Be, μg W^{-1}	24	20	16
C, g	13	7	6
C, μg s^{-1}	189	102	71
C, μg MJ^{-1}	87	35	24
C, μg W^{-1}	6.0	2.4	2.1

rate during JET-ILW1 can possibly be explained by C remaining from JET-C, or due to residual carbon impurities on top of the tiles. From JET-ILW1 to JET-ILW2 the C accumulation decreased by a factor of about 2 both in the absolute amount, and in terms of accumulation rates. The reduction of the C accumulation rate from JET-ILW2 to JET-ILW3 is less significant. The source of the remaining C could potentially be erosion of sides and back surfaces of JET divertor tiles, which consist of carbon fiber composite material not protected by W coating. Such erosion was previously suggested as the source of C accumulation in the shadowed areas of the divertor [20].

The absolute Be accumulation increased slightly from JET-ILW1 to JET-ILW2, and then decreased by ∼23% from JET-ILW2 to JET-ILW3. In terms of accumulation rates, the highest Be accumulation rate occurred in the JET-ILW2 campaign, while the smallest was in the JET-ILW3 campaign. However, normalizing by either total input energy or by average input power, one can see that the Be accumulation rate decreased steadily from one campaign to the next. This can likely be attributed to fresh Be tiles installed before JET-ILW1 adapting to plasma-wall interaction, with rough edges and surfaces eroding leading to a decrease of average erosion rate in JET-ILW2 and JET-ILW3.

The D accumulation remained roughly constant in absolute numbers in all three campaigns. The accumulation rate normalized by total input energy or average input power decreased from JET-ILW1 to JET-ILW2, but remained steady, even increasing slightly from JET-ILW2 to JET-ILW3. The decrease of accumulation rate from JET-ILW1 to JET-ILW2 corresponds to the decrease in C accumulation rate. Both Be and C deposition rates decreased from JET-ILW2 to JET-ILW3, while the D retention rate increased. This makes it hard to conclusively state whether co-deposition with Be or with C are the pre-dominant D retention mechanisms. The distribution of D in the divertor correlates well with the areas of largest Be content, which makes it probable that Be-D co-deposition is more significant than D-C co-deposition. The other significant channel of D retention is

Figure 5. Typical distribution of D in the near surface area of the outer divertor tile 8 (*s*-coordinate ≈1900). Green line—JET-ILW2, red line—JET-ILW3. Dashed vertical line indicate the interface between the W marker layer and the underlying Mo interlayer.

retention in the W protective coatings, where retention can be high due to the large number of defects in the coatings [21].

3.3. D depth distribution

A number of D depth profiling studies were performed in all three JET-ILW campaigns.

In all three campaigns, it was observed that D accumulated deep in W coatings (figure 5), with D concentrations of ∼1–2 at% observed consistently in the outer divertor through the whole W marker layer, up to depths of ∼3 μm. High concentrations of D were observed on the interface between the W marker coatings and the Mo interlayers. It can be speculated that such deep accumulation is due to the porous structure of the protective coating, where large numbers of trapping sites are present. Deep D accumulation was observed in the areas that likely underwent significant heat fluxes, such as tile 7 during JET-ILW3, indicating that W annealing was not effective in reducing the number of trap sites present.

This deep D accumulation indicates that in the bulk tungsten divertor tile 5 rather than plasma-produced W coatings, the total hydrogen accumulation is likely to be significantly lower. This was observed by comparing D depth profiles in neighboring lamellae of tile 5 with and without W marker coating (figure 6).

When comparing D depth profiles in tile 5 bulk W lamellae after JET-ILW1 and JET-ILW2, one can also see that after JET-ILW2, almost no D was observed in the area closest to the surface of the lamellae. At the end of JET-ILW2, ∼300 discharges with H instead of D were conducted, causing D to be removed from the near surface areas. The same effects could not be observed in the near surface area of tile 8, either due to its lower temperature during the discharges or smaller particle fluxes.
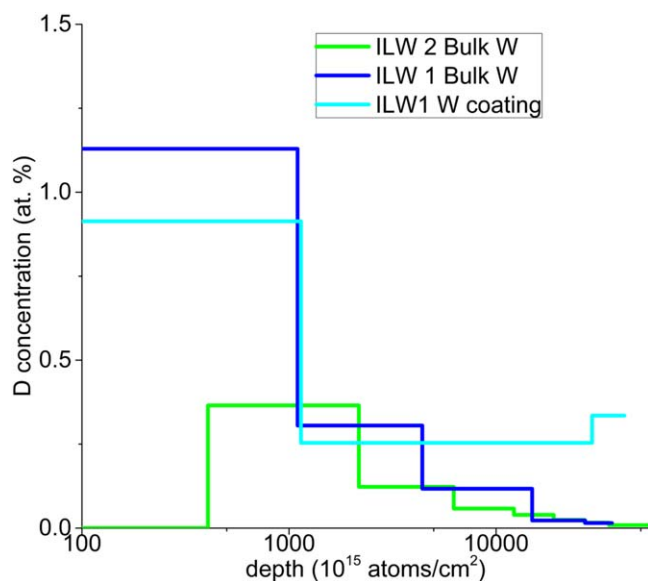
Figure 6. Typical distribution of D in the near surface area of the center divertor tile 5 (*s*-coordinate ≈1150). Green line—JET-ILW2 bulk W lamella without marker tile, dark blue line—JET-ILW1 bulk W lamella without marker tile, light blue line—JET-ILW1 bulk W lamella with a marker coating on top.

4. Summary

The erosion and deposition patterns in the JET divertor were studied and compared for the first three ILW campaigns using cutouts from divertor tiles. The following observations were made:

- The retention rate of D decreased from 13 μg s^{-1} in JET-ILW1 to 10 μg s^{-1} in JET-ILW3, the deposition rate for Be decreased from 771 to 544 μg s^{-1}, with a peak of 877 μg s^{-1} during JET-ILW2, and for C from 189 to 71 μg s^{-1}.
- The highest decrease is observed for the C deposition rate and can be probably explained by exhaustion of carbon sources as leftovers from the switch from JET-C to JET-ILW.
- The rate of material accumulation per input energy and per average input power decreased steadily from 24 μg W^{-1} for Be, 0.41 μg W^{-1} for D, and 6.0 μg W^{-1} for C in JET-ILW1 to 16 μg W^{-1} for Be, 0.31 μg W^{-1} for D, and 2.1 μg W^{-1} for C in JET-ILW3.
- The poloidal distributions of deposited material were similar in all three campaigns. The maximum of deposition was on top of tiles 0 and 1, in the region from ∼50 mm *s*-coordinate to ∼300 mm *s*-coordinate. This distribution is attributed to Be being transported into those areas from the SOL, and mainly remaining where it arrives into the divertor, without much further transport in the divertor itself. In the second and third ILW campaigns, where the strike-point distribution favored tiles 4 and 6, peaks of Be accumulation in those areas were also observed.

- Based on the Be and D distributions in the divertor, co-deposition with Be is probably the most significant channel of D retention.
- D was also retained deep inside tungsten protective layers in all campaigns relatively similarly. This retention is attributed primarily to the strong distortions, such as porosity, of the W coating providing a large amount of D trap sites. In bulk W this deep D accumulation is not observed.
- In both JET-ILW1 and JET-ILW2 campaigns, the erosion was strongest in the area of tile 5 near the strike point maximum. In both JET-ILW2 and JET-ILW3, erosion of W was observed in the outer divertor, on tiles 6 (only data for JET-ILW2 is available) and 7.
- Strong changes to the structure of W marker coating of the lower area of tile 7 in the outer divertor were observed. Such changes are likely due to either W and Mo layer interdiffusion under strong heat flux, or inhomogeneous erosion and redeposition of W leading to an increase in W layer roughness.

Acknowledgments

ORCID iDs

S Krat ⓘ https://orcid.org/0000-0001-6223-293X
M Mayer ⓘ https://orcid.org/0000-0002-5337-6963
S Brezinsek ⓘ https://orcid.org/0000-0002-7213-3326
K Heinola ⓘ https://orcid.org/0000-0002-0601-8274
A Widdowson ⓘ https://orcid.org/0000-0002-6805-8853

References

[1] Likonen J, Coad J P, Vainonen-Ahlgren E, Renvall T, Hole D E, Rubel M and Widdowson A 2007 Structural studies of deposited layers on JET MkII-SRP inner divertor tiles *J. Nucl. Mater.* **363–365** 190–5

[2] Roth J *et al* 2009 Recent analysis of key plasma wall interactions issues for ITER *J. Nucl. Mater.* **390–391** 1–9

[3] Krat S, Gasparyan Y, Pisarev A, Mayer M, von Toussaint U, Coad P and Widdowson A 2015 Hydrocarbon film deposition inside cavity samples in remote areas of the JET divertor during the 1999–2001 and 2005–2009 campaigns *J. Nucl. Mater.* **463** 822–6

[4] Matthews G F *et al* 2011 JET ITER-like wall—overview and experimental programme *Phys. Scr.* **T145** 014001

[5] Mertens P 2011 Detailed design of a solid tungsten divertor row for JET in relation to the physics goals *Phys. Scr.* **T145** 014002

[6] Baron-Wiechec A *et al* 2015 Global erosion and deposition patterns in JET with the ITER-like wall *J. Nucl. Mater.* **463** 157–61

[7] Mayer M *et al* 2016 Erosion and deposition in the JET divertor during the first ILW campaign *Phys. Scr.* **T167** 014051

[8] Krat S, Gasparyan Y, Pisarev A, Bykov I, Mayer M, de Saint Aubin G, Balden M, Lungu C P and Widdowson A 2015 Erosion at the inner wall of JET during the discharge campaign 2011–2012 in comparison with previous campaigns *J. Nucl. Mater.* **456** 106–10

[9] Beal J *et al* 2016 Deposition in the inner and outer corners of the JET divertor with carbon wall and metallic ITER-like wall *Phys. Scr.* **T167** 14052

[10] Heinola K *et al* 2016 Long-term fuel retention in JET ITER-like wall *Phys. Scr.* **T167** 014075

[11] Krat S, Mayer M and Porosnicu C 2015 The 9Be(p,p0)9Be, 9Be(p,d0)8Be, and 9Be(p,α0)6Li cross-sections for analytical purposes *Nucl. Instrum. Methods Phys. Res.* B **358** 72–81

[12] Gurbich A F 2016 SigmaCalc recent development and present status of the evaluated cross-sections for IBA *Nucl. Instrum. Methods Phys. Res.* B **371** 27–32

[13] Mayer M, Gauthier E, Sugiyama K and von Toussaint U 2009 Quantitative depth profiling of deuterium up to very large depths *Nucl. Instrum. Methods Phys. Res.* B **267** 506–12

[14] Alimov V K, Mayer M and Roth J 2005 Differential cross-section of the D(3He,p)4He nuclear reaction and depth profiling of deuterium up to large depths *Nucl. Instrum. Methods Phys. Res.* B **234** 169–75

[15] Johnston R L, Holmgren H D, Wolicki E A and Illsley E G 1958 Differential cross sections for the C12(He3,p)N14 Reaction *Phys. Rev.* **109** 884–7

[16] Barradas N P, Catarino N, Mateus R, Magalhães S, Alves E, Siketić Z and Radović I B 2015 Determination of the 9Be (3He,pi)11B (*i* = 0, 1, 2, 3) cross section at 135° in the energy range 1–2.5MeV *Nucl. Instrum. Methods Phys. Res.* B **346** 21–5

[17] Brezinsek S *et al* 2016 Characterisation of the deuterium recycling at the W divertor target plates in JET during steady-state plasma conditions and ELMs *Phys. Scr.* **T167** 014076

[18] Eckstein W 2007 Sputtering yields ed W Eckstein *Sputtering Part. Bombard. Top. Appl. Phys.* **110** 33–187

[19] Heinola K, Ahlgren T, Brezinsek S, Vuoriheimo T and Wiesen S 2019 Modelling of the effect of ELMs on fuel retention at the bulk W divertor of JET *Nucl. Mater. Energy* **19** 397–402

[20] Krat S, Mayer M, von Toussaint U, Coad P, Widdowson A, Gasparyan Y and Pisarev A 2017 Beryllium film deposition in cavity samples in remote areas of the JET divertor during the 2011–2012 ITER-like wall campaign *Nucl. Mater. Energy* **12** 548–52

[21] Ogorodnikova O V, Ruset C, Dellasega D, Pezzoli A, Passoni M, Sugiyama K, Gasparyan Y and Efimov V 2018 Deuterium retention in dense and disordered nanostructured tungsten coatings *J. Nucl. Mater.* **507** 226–40